Inner Shell Excitation Spectroscopy of Biphenyl and Substituted Biphenyls: Probing Ring−Ring Delocalization

Jian Wang, Glyn Cooper, David Tulumello, and Adam P. Hitchcock*

Department of Chemistry, McMaster University, Hamilton, Ontario, Canada L8S 4M1

Received: August 19, 2005; In Final Form: October 1, 2005

Quantitative optical oscillator strength spectra for C 1s excitation and ionization of gas-phase biphenyl, decafluorobiphenyl, and 2,2′-bis(bromomethyl)-1,1′-biphenyl have been derived from electron energy loss spectroscopy recorded under electric dipole dominated conditions. The C 1s X-ray absorption spectrum of hexaphenylbenzene has been recorded in the solid state. The C 1s spectral features are interpreted with the aid of ab initio calculations for core excitation of benzene, biphenyl, hexafluorobenzene, and decafluorobiphenyl. A weak feature at 287.7 eV in biphenyl is identified as a C 1s → π^*_{deloc} transition, characteristic of ring−ring delocalization. Its intensity and position are shown to be related to the average torsion angle and thus the extent of $\pi-\pi$-interaction between adjacent aromatic rings. The effects of perfluoro substitution on core excitation spectra are also characterized and discussed.

1. Introduction

The geometric and electronic structure of biphenyl and substituted biphenyls has attracted much interest over the years. The parent species was initially considered to be planar in the gas phase. In 1907, Kaufler[1] proposed a geometry in which the two rings were rigidly orthogonal. Both of these early views were disproved and the accepted geometry in which the rings are twisted relative to each other with large amplitude torsional modes has been established by a number of techniques, including studies of the optical activity of biphenyl derivatives.[2] The most recent electron diffraction studies have shown that the mean dihedral angle of gas-phase biphenyl is 44.4 ± 1.2°.[3] Apart from the experimental studies, intensive theoretical work has been carried out in the past decade in order to find a consistent optimized torsional angle for biphenyl.[4−9] However, the theoretical results are in only semiquantitative agreement with experiment; the best result gives a dihedral angle of ∼40° in the ground state, with a barrier to rotation of about 1.5 kcal/mol.[6,8,9] Calculations indicate that population of the π^* LUMO, as in formation of the ground state of the anion, results in the planar conformation being the most stable, while ionization of the π HOMO reduces the average dihedral angle to ∼20°.[6] Moreover, the geometry of biphenyl in the gas phase, solution, and the solid state differs.[10,11] Substituted biphenyls, particularly ortho or ortho disubstituted species, have a significantly increased dihedral angle.[12]

Clearly, the preferred conformation of a biphenyl system is determined by a delicate balance of a number of factors, and thus it is strongly dependent on the local environment. Biphenyls can be considered as a system of two interacting moieties with the electronic interactions between these two moieties being susceptible to modification by conformational changes.[13] Thus, in the fully planar configuration one would expect full delocalization of the π-system over the two rings, whereas in the 90° twist conformation in which the two phenyl rings are fully orthogonal, a description in terms of two independent, noninteracting π-systems would be more appropriate. The potential to control electronic communication between adjacent aromatic rings in polyparaphenylene systems by conformational changes at specific points along a string of aromatic rings linked by nominal C−C single bonds is being explored as a means for conductance switching in organic electronics.[14] Surface-tethered biphenyl structures are being devised and investigated for possible sensor applications.[15−17] Experimental methods to study the electronic structure of such systems, particularly with high spatial resolution, are of great interest. One of these is near-edge X-ray absorption fine structure (NEXAFS) microscopy, as implemented in X-ray photoemission electron microscopy (X-PEEM)[18] or scanning transmission X-ray microscopy (STXM).[19,20] To optimize NEXAFS microscopy for studies of systems involving linked aromatic rings, fundamental studies of the inner shell excitation spectroscopy of biphenyl and substituted-biphenyl molecules are required.

Inner shell excitation using X-ray absorption[21] or inner shell electron energy loss spectroscopy (ISEELS)[22,23] is a powerful probe of electronic structure. Here we have used ISEELS to record the inner shell electron energy loss spectra of gaseous biphenyl (**1**), decafluorobiphenyl (**2**), and 2,2′-bis(bromomethyl)-1,1′-biphenyl (**3**). In addition, we have measured the C 1s NEXAFS spectrum of solid hexaphenylbenzene (**4**). With regard to closely related work, a high-resolution NEXAFS study of gaseous biphenyl was reported recently.[24] That study is complementary to the present work, since it only dealt with the vibrational band structure of the lowest energy C 1s → π^* transition at 285 eV. Otherwise, to our knowledge, this is the first report of the inner shell spectra of these four species. These molecules were selected for study in order to investigate the effect on the C 1s spectrum of varying degrees of π-delocalization between two phenyl rings coupled by a nominal C−C single bond. The degree of delocalization is expected to change because these systems have different mean torsional angles. In particular, species with bulky ortho substituents have a larger torsional angle and thus are expected to have reduced π-delocalization. The theme of "geometric control of delocalization" has been explored in core excitation studies of other systems.[25,26]

* Corresponding author. Office: (905) 525-9140, Ext. 24749. Fax: (905) 521-2773. E-mail: aph@mcmaster.ca.

10.1021/jp054693n CCC: $30.25
Published on Web 11/12/2005

Delocalization across the peptide bond may be an important determinant of peptide conformation, and thus an improved understanding of the links between delocalization and core excitation spectra may assist development of core excitation as a more powerful probe of proteins and peptides.[27]

Another theme of this study is the perfluoro effect, which refers to the influence of extensive fluorine substitution in spectroscopies, in this case, core excitation spectroscopy, in particular of aromatic species such as biphenyls. Fluorine substitution causes large core level chemical shifts and also characteristic shifts in the unoccupied electronic structure that are manifested in specific ways in C 1s spectra. This theme has been explored earlier in systematic studies of perfluorinated alkanes, alkenes,[28] and benzenes.[29] A better understanding of the perfluoro effect[30] will assist analytical applications of inner shell excitation spectroscopies and associated spectromicroscopies for studies of fluorinated organic materials.

The inner shell spectra are interpreted with the help of ab initio GSCF3 calculations[31,32] and experiment−calculation comparisons of biphenyl and decafluorobiphenyl with respect to benzene[33] and hexafluorobenzene.[28,29] Calculations of the dependence of the C 1s spectra on twist angle are used to predict the spectral consequences of delocalization. Comparisons of the experimental spectra of biphenyl and benzene are used to show that these signals actually exist.

2. Experimental Section

2.1. Inner Shell Electron Energy Loss Spectroscopy. Biphenyl (**1**), decafluorobiphenyl (**2**), and 2,2′-bis(bromomethyl)-1,1′-biphenyl (**3**) were obtained from Sigma Aldrich in the form of white powder crystals for **1** and **3** and white needle crystals for **2**, with stated purities of better than 99.5%, 97%, and 99%, respectively. The samples were used without further purification.

In ISEELS, core electronic excitation occurs by inelastic collision of a high-energy electron beam (2.5 keV plus the energy loss) with a molecule. An excited state is created by the transfer of energy from the incident electron. By measuring the distributions of energy losses of inelastically scattered electrons, a spectrum is produced from which the characteristics of the molecule can be deduced. The apparatus and techniques have been described elsewhere.[23] For the gas-phase ISEELS measurements, samples **1** and **3** were introduced directly into the collision chamber of the ISEELS spectrometer. Biphenyl gave adequate vapor pressure at room temperature while **3** required heating the collision cell to ∼80 °C. **2** is volatile so it was introduced through a leak valve.

The ISEELS spectra were acquired using a 2° scattering angle (to avoid main beam background) and high electron impact energy (2.5 keV + energy loss), conditions under which electric dipole transitions are known to dominate.[23] The energy resolution is dependent on the electron beam current and analyzer pass energy. With the pass energy used, it was 0.9 eV full width at half-maximum (fwhm) at 25 μA beam current and 0.5 eV fwhm for 2 μA beam current. The energy scales were calibrated by recording the spectrum of a mixture of the analyte and CO. The C 1s spectra reported herein are combinations of low- and high-current spectra recorded between 278 and 325 eV. They were background subtracted using a fit of the function $a(E-b)^c$ to the preedge region. The so-isolated C 1s signal was then converted to a quantitative oscillator strength scale by matching to the standard oscillator strength of a single carbon atom[22,23,34] outside the structured near-edge region.

2.2. X-ray Absorption Spectroscopy. Hexaphenylbenzene (**4**) was prepared by Diels−Alder reaction from tetraphenylcyclopentadienone and diphenylacetylene[35] and the product was purified by recrystallization from dichloromethane. Its structure was confirmed by mass spectrometry. The STXM sample was prepared by solvent casting from a millimolar toluene solution of **4** on a 100 nm silicon nitride membrane window (Silson plc). Rapid crystallization occurred as the solvent evaporated. STXM was used to image and thus identify a crystal with suitable thickness. The X-ray absorption spectrum of **4** was recorded in transmission mode from very thin (∼100 nm) crystals using the scanning transmission X-ray microscope (STXM)[36] at beamline 5.3.2[37] at the Advanced Light Source. Acquisition and analysis procedures have been described in detail elsewhere.[38] Spectra were acquired using the image sequence technique.[39] The as-recorded transmitted signal was converted to optical density using the spectrum of the incident flux passing through an adjacent bare area of the silicon nitride window. This spectrum was then converted to an absolute optical oscillator strength scale using the elemental response reported in the literature.[34]

2.3. Ab Initio Calculations. Calculations were performed using GSCF3 (Gaussian Self-Consistent Field, version 3),[31,32] which is an ab initio code designed specifically to predict inner shell excitation and ionization spectra. The program uses the Hartree−Fock-SCF approach and explicit core holes to solve for the energies and molecular orbitals of the system under investigation. There are three steps for the calculation. In step one, the eigenvectors (MOs) and eigenvalues of the ground state are calculated, and the core MO that will lose the electron is identified. In the second step, the core ion state is computed by removing the user-specified core electron and allowing the system to relax and reorganize in the presence of the core hole. The difference in the total energy of the core-ionized and ground state (ΔSCF) is the calculated core level ionization potential (IP), which tracks chemical changes within ∼0.5 eV, but is typically high by 2 ± 1 eV. The third step computes excitation energies and transition probabilities for all one-electron core → valence excitations using the improved virtual orbital (IVO) approximation. IVO assumes the energy of a core excited state is given by the sum of the computed ΔSCF IP plus the eigenvalue (ϵ) of the upper orbital in the core-ionized state. The energies and optical oscillator strengths determined by the GSCF3 calculation for a given core excitation site are used to generate the simulated core excitation spectrum for that site by summing Gaussian lines at an energy given by the term value ($TV = IP - E = -\epsilon$), an area given by the oscillator strength for excitation to each improved virtual orbital and a width chosen as a function of the term value. For the simulated spectra, the Gaussian widths used were 0.8 eV for TV > 2 eV, 2.0 eV for 2 eV > TV > −2 eV, 4.0 eV for −2 eV > TV > −10 eV, and 6.0 eV for TV < −10 eV. Since there are multiple chemically distinct sites in the biphenyl species, the spectrum for each site was computed, and then the spectrum of the full molecule was calculated from the stoichiometrically weighted sum. For instance, there are four carbon sites in biphenyl (see Figure 1 for labeling). For each carbon site, the calculated IP was used to set the energy scale of the simulated C 1s oscillator strength spectrum. The final calculated C 1s spectrum of biphenyl was generated from the weighted sum of the computed spectra for all carbon sites, i.e., $(2C_1 + 4(C_2 + C_3 + C_4)/12)$.

The basis sets used in the calculations were those of Huzinaga et al.[40] Specifically, the HTS6X (41121/2111) contracted Gaussian-type extended basis set was used for carbon and fluorine atoms with a localized core hole, while the HTS4X (53/4) basis set was chosen for noncore hole carbon and fluorine

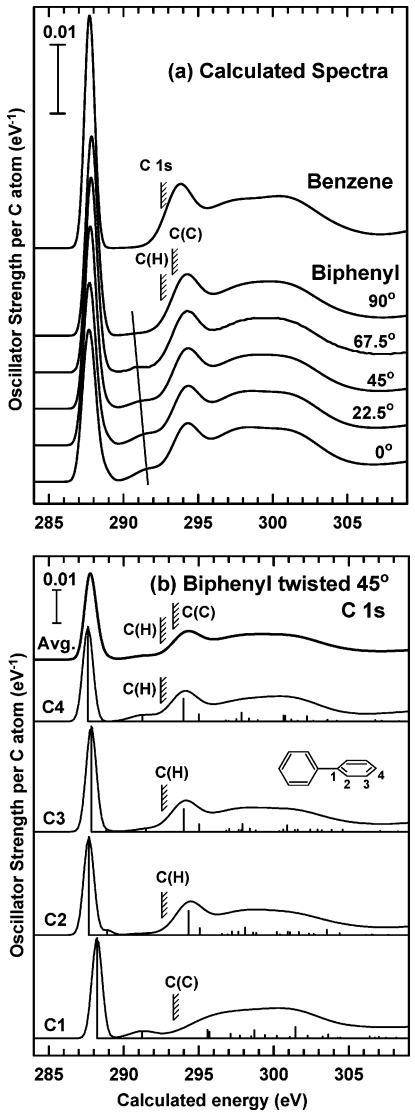

Figure 1. (a) GSCF3-computed C 1s spectra of benzene and biphenyl with torsional angles varying from 0° to 90°. The hatched lines indicate the computed IPs. The line indicates the π^*_{deloc} feature (see the text). (b) Site specific components for the computed spectrum of the 45° conformation.

atoms, and the HTS3X (6) basis set was used for hydrogen atoms. Two-membered exponents (*d*-polarization functions) were also used for core hole atoms to achieve better agreement of the computational and experimental results. The geometries of biphenyl, benzene, decafluorobiphenyl, and hexafluorobenzene used in the calculation (listed in the Supporting Information, Table S1) were computed by energy minimization with a 6-31G* basis using Spartan 04 version 1.01. These calculations indicate a planar conformation for all species. The twisted conformations of biphenyl and decafluorobiphenyl were derived from these planar geometries by rigidly twisting the dihedral angle of the two phenyl rings.

3. Results

3.1. Calculated C 1s Spectrum of Biphenyl: Conformational Dependence. Figure 1a shows the calculated C 1s spectrum of benzene in comparison to those of five different conformations of biphenyl with torsional angles varying from 0° to 90°. Figure 1b presents the detailed site-by-site spectra for the 45° conformation. The computed eigenvalues, IPs, and oscillator strengths of selected transitions for 45°-twisted biphenyl are listed in Table 1, along with the computational results for benzene. The Supporting Information (Table S2) has a more extensive listing of information from the GSCF3 calculations. Since the mean torsional angle of biphenyl in the gas phase is known to be 44.4 ± 1.2°,[3] the simulated C 1s spectrum of 45°-twisted biphenyl is used for further comparison with experimental results. This is considered meaningful since torsional motion is much slower than the time scale of core excitation, and thus, the excitation takes place at the specific conformation a molecule has at the time of the electronic excitation. Thus, although the most stable geometry of (C $1s^{-1}$, $1\pi^*$) excited states of biphenyl might be planar, the relevant geometry for this spectroscopy is that of the ground state. These biphenyl species have rather low torsional barriers (e.g. ~6 kJ/mol for biphenyl[41]) and thus an ensemble of molecules will have a Boltzmann distribution of torsional angles characteristic of the sample temperature (~25 °C). The Boltzmann populations for 0°, 22.5°, 45°, 67.5°, and 90° conformations of biphenyl at 25 °C are 5.2%, 17.5%, 58.7%, 14.3%, and 4.3%, respectively. Thus the minimum energy conformation (45°) dominates the distribution. For substituted biphenyls, which have a larger torsional barrier, the fractional population in the minimum energy conformation will be even larger.

TABLE 1: Selected Eigenvalues, Oscillator Strengths, and Orbital Characters for Computed Core-Excited States of 45°-Twisted Biphenyl and Benzene

site	IP	character	ϵ (eV)	f (10^{-2})
		Biphenyl Twisted 45°		
C1	293.191	$1\pi^*(b_1)$	−4.97	2.48
		$1\pi^*(a)$	−3.41	0.00
		$1\pi^*(b_3)$	−1.97	0.42
		$1\pi^*(b_2)$	−1.67	0.00
		$2\pi^*$ (b_1)	2.39	1.03
		σ^*(C−C) (inter ring)	2.52	0.80
C2	292.402	$1\pi^*(b_1)$	−4.73	2.43
		$1\pi^*(a)$	−3.50	0.12
		$1\pi^*(b_2)$	−1.46	0.03
		$1\pi^*(b_3)$	−1.32	0.04
		$2\pi^*$ (b_1)	2.66	0.85
C3	292.445	$1\pi^*(b_1)$	−4.61	2.61
		$1\pi^*(a)$	−3.62	0.03
		$1\pi^*(b_3)$	−0.96	0.13
		$1\pi^*(b_2)$	−0.94	0.01
		$2\pi^*(b_1)$	2.58	0.92
C4	292.338	$1\pi^*(b_1)$	−4.72	2.34
		$1\pi^*(a)$	−3.21	0.00
		$1\pi^*(b_3)$	−1.09	0.36
		$1\pi^*(b_2)$	−0.96	0.00
		$2\pi^*(b_1)$	2.67	0.90
		σ^*(C−H)	4.47	0.13
		Benzene		
C	292.536	$1\pi^*e_{2u}$	−4.81	2.72
		$1\pi^*e_{2u}$	−3.52	0.00
		σ^*(C−H)	1.14	1.38
		$2\pi^*b_{2g}$	2.50	1.03

The computed spectrum of biphenyl is dominated by the strong C 1s → $1\pi^*(b_1)$ transition at 285.2 eV. (Note, for ease in correlating to experimental energies, the shift used to align the calculated and experimental spectra has been incorporated into the energies cited in the text. The actual value for the computed core excitation energy can be obtained by adding the shift listed in the figure caption, or by adding the eigenvalues and the IP listed in Table 1. The symmetry labels are those for the molecular orbitals in the optimally twisted conformation if not specified.) At somewhat higher energy there is a weak feature at ~288 eV arising from C 1s → $1\pi^*(b_3)$ excitation, which is marked by a line in Figure 1a. The energy and intensity of this feature is strongly dependent on the torsional angle. It

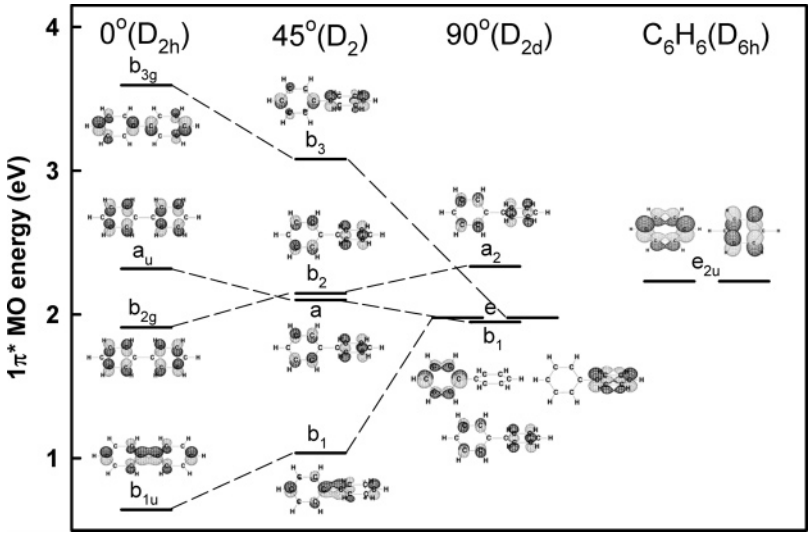

Figure 2. Energy level diagram and plots of the $1\pi^*$ (e_{2u}-derived) molecular orbitals of the ground state of planar, 45°-twisted, and 90°-twisted biphenyl and benzene.

is strongest in the planar conformation and disappears in the 90°-twisted geometry. This feature is the "signature" of π-delocalization.

Owing to ring−ring interaction and reduction of symmetry, the two degenerate $1\pi^*(e_{2u})$ molecular orbitals (MO) in benzene combine to form four $1\pi^*$ MOs in biphenyl. Figure 2 shows the GSCF3-computed ground-state energy levels and MO plots for these four $1\pi^*$ orbitals for planar, 45°-twisted, and 90°-twisted biphenyl. The energy and plots for the $1\pi^*(e_{2u})$ MO of benzene are also shown for reference. To avoid distortion of the ground-state MO energy levels and plots, we have removed the polarization functions and used a HTS4X (53/4) basis set for the core hole atoms to get the results shown in Figure 2. Symmetry labels and correlation of the MOs between different conformations are also indicated in Figure 2. Inspection of the MO plots for the planar and 45° conformations indicates that there is extensive interaction between the two rings due to delocalization across the inter-ring C−C bond. For the 45°-twisted biphenyl, the transition oscillator strengths for different carbon sites are listed in Table 1, and also, in more detail, in Table S2 (Supporting Information). Electric dipole excitations are allowed from one or the other of the C 1s orbitals to the $1\pi^*(b_1)$, $1\pi^*(b_3)$, and $1\pi^*$(a) MOs, whereas all C 1s excitations to $1\pi^*(b_2)$ are forbidden. The $1\pi^*(b_2)$ and $1\pi^*$(a) MOs are very close in energy and become almost degenerate at a torsional angle of 45°. Of the four $1\pi^*$ orbitals in 45°-twisted biphenyl, the lowest energy $1\pi^*(b_1)$ level has some bonding character, while the highest energy $1\pi^*(b_3)$ level has some antibonding character across the inter-ring C−C bond. The energy separation of these two levels is clearly related to the extent of delocalization, since the contributions on each ring and the energy separation decrease systematically as the torsional angle increases. Overall the main effect of delocalization across the two rings is to split the two $1\pi^*$ (e_{2u}) levels in two noninteracting benzenes into effectively three levels, with the $1\pi^*(b_1)$ at lowest energy, the $1\pi^*(b_3)$ at highest energy, and the $1\pi^*(b_2)$ and $1\pi^*$-(a) MOs at about the same energy as in the weakly interacting system. The dipole-allowed C 1s → $1\pi^*(b_3)$ transitions should be seen ~3 eV above the main C 1s → $1\pi^*(b_1)$ transition. The partly dipole-allowed C 1s → $1\pi^*$(a) transition should create a weak shoulder on the higher energy side of the main $1\pi^*(b_1)$ feature, which may be too weak to see experimentally.

The energies for C 1s → $1\pi^*$ transitions at different C 1s sites (Tables 1 and S2) are not always in the same energetic sequence as that of the corresponding MOs in the ground state. This is a strong consequence of site-specific core hole localization effects.[21,28,42] When a C 1s electron is excited, the localized C 1s core hole pulls down the energy of the C 2p level of the excited carbon atom by ~2 eV relative to that for the 2p level of other carbon atoms. Thus the lowest π^* orbital becomes concentrated at the core excited carbon atom. The energy of the lowest ($C\ 1s^{-1}$, π^*) state is determined by the electronic structure at the core excited carbon atom and the relaxation of the rest of the valence electron distribution in the presence of the localized core hole. The extent of core-hole relaxation is site specific in aromatic systems.[42] The transition intensity, which is largely determined by the contributions to the upper MO of the $2p\pi^*$ orbital on the core excited atom, is strongly concentrated in the lowest energy 1s → π^* transition. GSCF3 core excitation calculations use an explicit localized core hole, allow the system to relax in its presence, and thus generally give good agreement with experiment. In contrast to the situation of fully or partially delocalized $1\pi^*$ levels in the planar and 45°-twisted conformations of biphenyl, when the C−C bond is twisted 90°, the $1\pi^*$ MOs on each ring are energetically equivalent, resulting in energies and spatial distributions that are very similar to those of benzene (Figure 2).

3.2. Experimental C 1s Spectrum of Biphenyl (Gas). Figure 3 presents the oscillator spectrum for C 1s excitation of biphenyl derived from dipole-regime ISEELS, compared to the experimental spectrum of benzene. Figure 3 also plots the calculated C 1s spectrum of benzene and 45°-twisted biphenyl. The energies, term values, and proposed assignments of the observed experimental spectral features are indicated in Table 2. To compare the experimental and calculated spectra, the calculated C 1s spectrum was shifted to higher energy by 2.5 eV to obtain the best match in the low-energy π^* region where the calculations are most meaningful. This shift reflects limitations of GSCF3 calculations, which typically overestimate core level IPs by 2−3 eV. When this shift is applied, the peak positions and overall shapes of the computed spectra are reasonably close to the experimental spectra, although there are additional features in the 287−291 eV region in the experimental spectrum. The latter are Rydberg excitations, which are not included in the GSCF3 calculations reported in this work.

The GSCF3 calculations (Tables 1 and S2) provide information about the principal character of the upper MO of each transition. This information was used to support the spectral

TABLE 2: Energies (*E*, eV), Term Values (TV, eV), and Assignments of C 1s Spectral Features of Benzene, Biphenyl (1), 2,2′-Bis(bromomethyl)-1,1′-biphenyl) (3), and Hexaphenylbenzene (4)

benzene[a]		**1**		**3**		**4**		assignments (final orbital)	
E	TV	E	TV	E	TV	E	TV	C−H	C−C
285.15	5.1	285.26[b]	4.7	285.24[b]	4.8	285.18[c]	4.8	1π*	1π*
287.2	3.1	287.5	2.5	287.5	2.5	287.4	2.6	3s/σ*(C−H)	3s
		287.7						1$\pi^*_{deloc}(b_3)$	
289.1	1.2	289.2	0.8	289.4	0.6	289.0	1.0	4p/2π*	4p/2π*
290.3[d]		290.0[e]		290.0[f]		290.0[f]		IP	
		290.3[e]		290.3[f]		290.3[f]			IP
290.6	−0.3	290.7	−0.7	290.6	−0.6	290.1	−0.1		
						292.0	−2.0		σ*
293.6	−3.3	293.8	−3.8	293.7	−3.7	293.5	−3.5	σ*(C−C) (ring)	σ*(C−C) (ring)
						295.3	−5.0		σ*(C−C)
299.3	−9.0	300.2	−10.2	300.4	−10.4	298.6	−8.6	σ*(C−C) (ring)	σ*(C−C)
302.6	−12.3	303.2	−13.2	302.8	−12.8	303.4	−13.4	σ*(C−C) (ring)	

[a] Data also reported in ref 29. [b] Calibration: biphenyl = −2.14(6) eV, 2,2′-bis(bromomethyl)-1,1′-biphenyl = −2.16(6) eV relative to the C 1s → π* transition of CO (287.40(2) eV[50]). [c] Based on calibration of the STXM energy scale to Rydberg transitions in CO_2 (accurate to 0.04 eV). [d] Ionization potential (IP) of C_6H_6 is taken from X-ray photoelectron spectroscopy.[51] [e] IPs of biphenyl are taken from X-ray photoelectron spectroscopy.[24] [f] IPs of 2,2′-bis(bromomethyl)-1,1′-biphenyl and hexaphenylbenzene (s) are assumed to be the same as those of biphenyl.

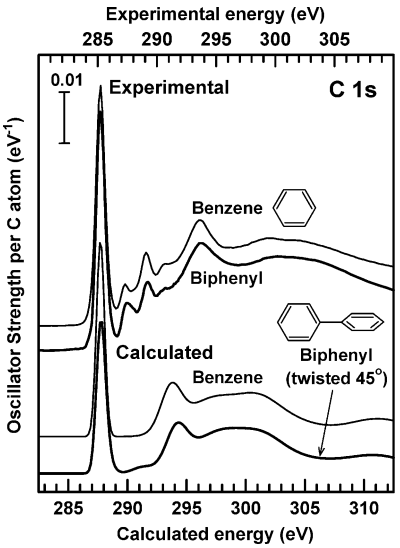

Figure 3. (Upper) Experimental C 1s oscillator strength spectra of biphenyl compared to that of benzene. Both spectra are derived from dipole regime inner shell electron energy loss spectra recorded with 2.5 keV impact energy and 2° scattering angle. (Lower) GSCF3 calculated spectra of benzene and 45°-twisted biphenyl. Offsets are used for clarity. The energy scale for the calculated spectrum has been shifted by −2.5 eV to align the 1π* feature with its experimental counterpart.

assignments listed in Table 2. The main peak at 285 eV is the lowest energy component of the 1π* states, the C 1s → 1π*-(b_1) transition. The features at 287.5 and 289.2 eV are assigned to C 1s → 3s and C 1s → 4p Rydberg transitions on the basis of their term values and the assignment of similar features in the C 1s spectrum of benzene.[28,29,33,43] While the Rydberg features dominate, a close comparison of the spectra of biphenyl and benzene in the 287−289 eV region indicates a difference in spectral shape. In particular, biphenyl has an additional signal at 287.7 eV, on the high energy side of the 3s Rydberg transition. This is interpreted as the C 1s → 1$\pi^*(b_3)$ transition, which has been identified in the torsion angle dependent calculations as the C 1s → $\pi^*_{delocal}$ feature specific to the ring−ring π-interaction. The upper level of the transition C 1s → 3s may also have some σ^*_{CH} character.[44] The peak at 289.2 eV may also be assigned to C 1s → 2π* transitions, as in benzene,[28] although the GSCF3 calculations give a larger term value for the 2π* MOs, as did earlier ab initio calculations for benzene.[45] The peaks at 294 and 300 eV are assigned to C 1s → σ*(C═C) (ring) transitions,[28] on the basis of bond length correlation considerations[21] and the results of MS-Xα calculations.[33]

Superficially, it appears that the C 1s spectra of biphenyl and benzene are very similar. However, a more careful examination reveals the changes predicted by the calculations. Within the building block approach, the spectrum of 90°-twisted biphenyl should be similar to that of benzene, aside perhaps for some minor changes associated with converting two C−H bonds into a C−C bond. On the other hand, if there are spectral observables associated with π*-delocalization, these should be discernible in the *difference* between the spectra of planar biphenyl and benzene. Figure 4a shows the difference between the experimental spectrum of biphenyl and benzene and the difference between the calculated spectrum of the 45° conformation of biphenyl and benzene. These difference signals are quite similar in shape and relative positions of features. The large derivative type signal at 285 eV is caused by a shift in energy of the main C 1s → π* transitions between biphenyl and benzene. At about 3 eV higher energy, there is a peak (at 287.7 eV experimental and 291.2 eV calculated, indicated by the dashed vertical line in Figure 4a) that is attributed to a C 1s → $\pi^*_{deloc}(b_3)$ transition, which reflects the π-delocalization between the two phenyl rings. In the calculation, the position and intensity of this feature evolves systematically with the biphenyl twist angle, as shown in Figure 4b. The π^*_{deloc} peak is strongest in the difference between the spectra of the planar and 90°-twisted biphenyl. It is not seen in the difference between the spectra of 90°-twisted biphenyl and benzene. According to the calculations, the C 1s → π^*_{deloc} transition is in fact the C 1s → 1$\pi^*(b_3)$ excitation, with that level arising from splitting of the1π* MO due to delocalization over the two phenyl rings.

3.3. C 1s Spectrum of Hexafluorobenzene and Decafluorobiphenyl. The mean torsional angle of solid decafluorobiphenyl was determined to be 59.7° by X-ray diffraction,[46] while a mean torsional angle of 55° was calculated for the gas phase.[7] When this information is combined with the electron diffraction result of a mean torsional angle of 60° for gas-phase 2,2′-difluorobiphenyl,[47] the estimated mean torsional angle of gas-phase decafluorobiphenyl is ∼60°, very similar to that of the solid. This is reasonable since the torsional angle is largely dependent on the ortho substituents for biphenyl systems.[7] Furthermore, calculations have predicted a rotation barrier of 25−30 kcal/mol for decafluorobiphenyl,[7] which will make the lowest energy 60° conformation dominate the conformation distribution at room temperature.

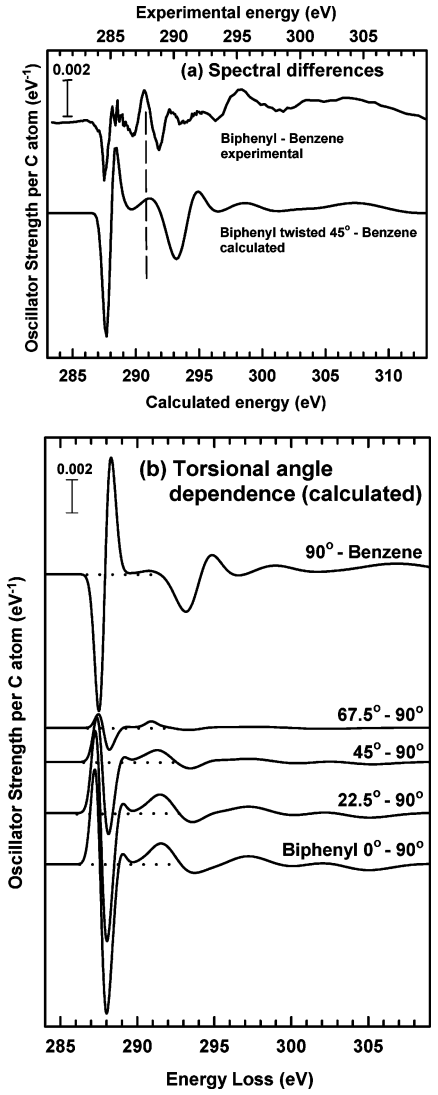

Figure 4. (a) Difference of the experimental C 1s spectra of biphenyl and benzene, in comparison to the difference in the calculated C 1s spectra of 45°-twisted biphenyl and benzene. (b) Difference of the calculated spectrum of 90°-twisted biphenyl with respect to those of other conformations, as well as the difference of the calculated spectra of 90°-twisted biphenyl and benzene.

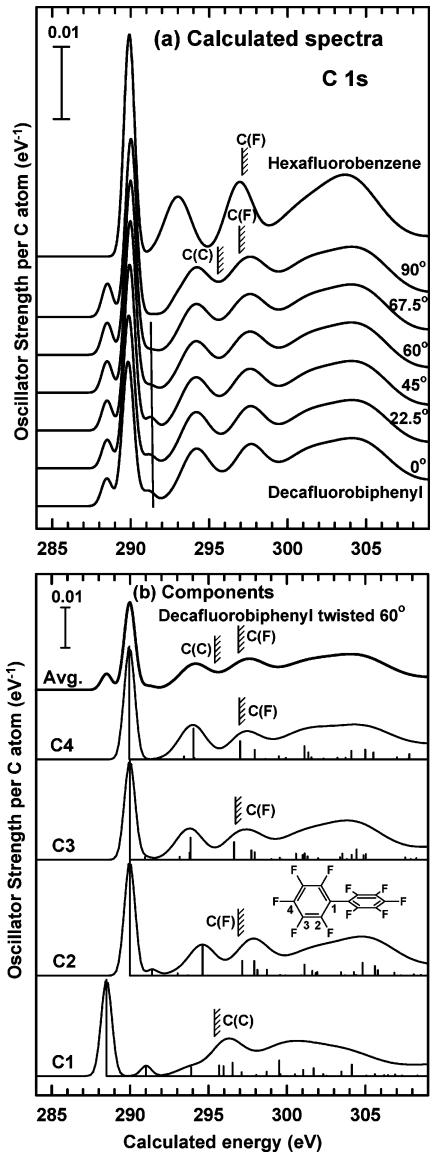

Figure 5. (a) Computed spectra of hexafluorobenzene and decafluorobiphenyl with torsional angles varying from 0° to 90°. The hatched lines indicate the computed IPs. The line indicates the π^*_{deloc} feature (see the text). (b) Site-specific components for the computed spectrum of the 60° conformation of decafluorobiphenyl.

Figure 5a shows the calculated C 1s spectra of hexafluorobenzene and that of six conformations of decafluorobiphenyl with torsional angles varying from 0° to 90°. Figure 5b presents the site-specific contributions to the computed spectrum of the 60° conformation. The computed eigenvalues, IPs, and oscillator strengths of selected transitions for 60°-twisted decafluorobiphenyl and hexafluorobenzene are listed in Table 3. Table S3 of the Supporting Information is a more extensive listing of the information from the GSCF3 calculations. Figure 6 displays the GSCF3-calculated $1\pi^*$ energies and MO plots of planar, 60°-twisted, and 90°-twisted decafluorobiphenyl, as well as those of hexafluorobenzene. These MO plots indicate that there is extensive delocalization across the two rings through the inter-ring C−C bond in the planar conformation. As in biphenyl, C 1s $\rightarrow$ $1\pi^*(b_3)$ transitions, overlapped with C 1s $\rightarrow$ $1\pi^*$(a) transitions, create a π^*_{deloc} feature ∼1.5 eV above the main C 1s $\rightarrow$ $1\pi^*$ feature (indicated by the line in Figure 5a). When the π^*-delocalization between the two phenyl rings is disrupted, as in 90°-twisted decafluorobiphenyl, this higher energy C 1s $\rightarrow$ π^*_{deloc} transition disappears, exactly analogous to the situation in biphenyl. Twisting about the C−C bond between the two rings reduces the π^*-delocalization, which appears as systematic energy and intensity shifts in the computed spectra. The energies of the C 1s(C−C) $\rightarrow$ $1\pi^*_{deloc}(b_3)$ and C 1s(C_2) $\rightarrow$ π^*(a) transitions in the 60°-twisted conformation are calculated to be ∼291 eV, corresponding to ∼289 eV experimentally. Relative to biphenyl, the C 1s spectrum of decafluorobiphenyl is complicated by the overlap of transitions associated with the C 1s(C−F) and C 1s(C−C) core levels, which are separated by ∼1.5 eV. Thus the two π^*_{deloc} features that are expected will be much harder to identify experimentally.

Figure 7 presents the experimental C 1s oscillator strength spectra of hexafluorbenzene and decafluorobiphenyl derived from dipole-regime ISEELS. Figure 7 also plots the calculated C 1s spectra of hexafluorbenzene and 60°-twisted decafluorobiphenyl. The calculated C 1s spectrum of decafluorobiphenyl was shifted −2.0 eV to align the computed C 1s $\rightarrow$ $1\pi^*(b_1)$ feature with its experimental counterpart. The computed MO character of the upper orbitals of the transitions are used to help assign the experimental C 1s ISEELS spectrum of decafluorobiphenyl. The energies, term values, and proposed assignments

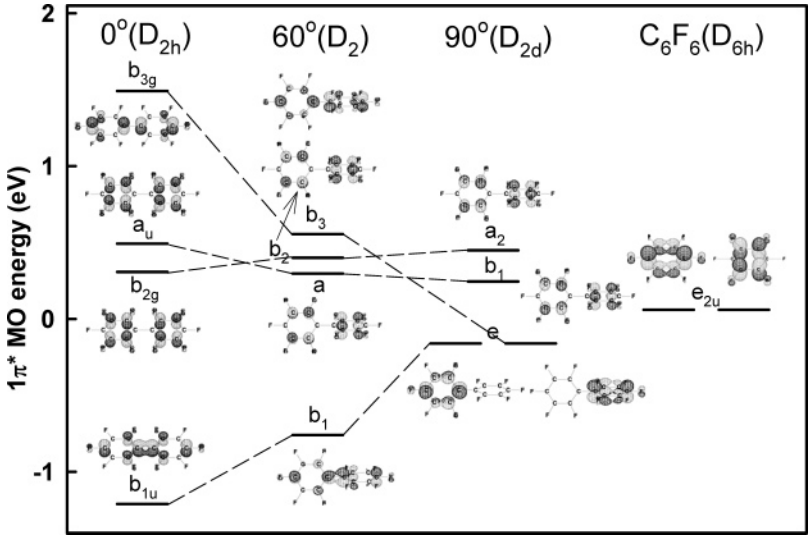

Figure 6. Energy level diagram and plots of the $1\pi^*$ (e_{2u}-derived) molecular orbitals of the ground state of planar, 60°-twisted, and 90°-twisted decafluorobiphenyl and hexafluorobenzene.

TABLE 3: Selected Eigenvalues, Oscillator Strengths, and Orbital Characters for Computed C 1s Core-excited States of 60°-Twisted Decafluorobiphenyl and hexafluorobenzene

site	IP	character	ϵ (eV)	f (10^{-2})
		Decafluorobiphenyl Twisted 60°		
C1	295.352	$1\pi^*(b_1)$	−6.86	2.13
		$1\pi^*(a)$	−5.09	0.00
		$1\pi^*(b_3)$	−4.33	0.23
		$1\pi^*(b_2)$	−3.41	0.00
		σ^*(C−C) (inter ring)	−1.46	0.48
		$2\pi^*(b_1)$	0.33	0.58
		σ^*(C−F)	0.60	0.53
		σ^*(C−F)	1.18	0.72
		σ^*(C−F)	4.15	1.70
C2	296.822	$1\pi^*(b_1)$	−6.84	2.52
		$1\pi^*(a)$	−5.42	0.13
		$1\pi^*(b_3)$	−3.78	0.12
		$1\pi^*(b_2)$	−3.14	0.01
		σ^*(C−F)	−2.19	1.67
		$2\pi^*(b_1)$	0.32	0.81
		σ^*(C−F)	1.09	0.81
		σ^*(C−F)	4.28	1.22
		σ^*(C−F)	4.80	0.51
C3	296.514	$1\pi^*(b_1)$	−6.53	2.18
		$1\pi^*(a)$	−5.56	0.07
		$1\pi^*(b_3)$	−3.36	0.16
		$1\pi^*(b_2)$	−2.72	0.40
		σ^*(C−F)	−2.66	1.21
		$2\pi^*(b_1)$	0.11	0.97
		σ^*(C−F)	1.22	0.53
		σ^*(C−F)	4.07	0.68
		σ^*(C−F)	4.81	0.38
C4	296.823	$1\pi^*(b_1)$	−6.87	2.49
		$1\pi^*(a)$	−5.15	0.00
		$1\pi^*(b_3)$	−3.38	0.17
		σ^*(C−F)	−2.78	1.70
		$1\pi^*(b_2)$	−2.72	0.07
		$2\pi^*(b_1)$	0.20	1.01
		σ^*(C−F)	1.13	0.53
		σ^*(C−F)	2.66	0.36
		σ^*(C−F)	4.29	1.45
		Hexafluorobenzene		
C	297.016	$1\pi^*e_{2u}$	−7.11	2.50
		$1\pi^*e_{2u}$	−5.72	0.00
		σ^*(C−F)	−4.01	1.69
		σ^*(C−F)	−0.29	0.99
		$2\pi^*b_{2g}$	0.02	0.95
		σ^*(C−F)	0.33	0.10
		σ^*(C−F)	3.39	1.62

of the experimental spectral features of these two species are summarized in Table 4. Comparing the experimental and the 60° computed spectra, there is good agreement in the shape

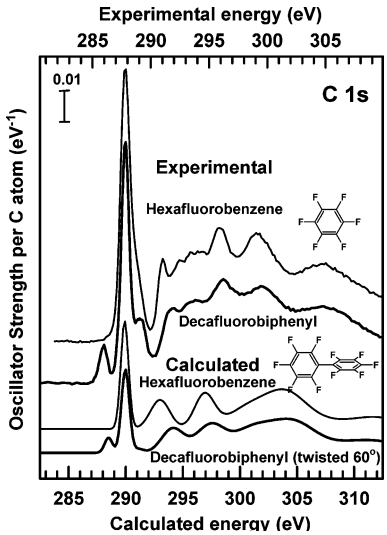

Figure 7. (Upper) C 1s oscillator strength spectra of decafluorobiphenyl compared to that of hexafluorobenzene. (Lower) GSCF3-calculated spectra of hexafluorobenzene and the 60°-twisted decafluorobiphenyl. Offsets are used for clarity. The energy scale for the calculated spectrum has been shifted by −2.0 eV to align the $1\pi^*$ feature with its experimental counterpart.

and relative position of the main spectral features. In particular, the computed spectrum predicts the weak π^*_{deloc} feature and the σ^*(C−F) feature at ∼294 eV. The lowest energy feature at 286.0 eV is assigned to C 1s(C−C) → $1\pi^*(b_1)$ transitions at site C_1. This feature is at low energy because C_1 is only bonded to other carbon atoms and thus its C 1s level is energetically above that of the C_2, C_3, and C_4 carbon atoms, which are bonded to a fluorine atom. The second feature at 287.8 eV is the main C 1s(C−F) → $1\pi^*(b_1)$ transitions at the C_2, C_3, and C_4 carbon atoms. The third feature at 289 eV is assigned mainly to C 1s → σ^*(C−F) transitions, as in hexafluorobenzene.[29] However, this feature may also be associated partly with C 1s → $1\pi^*_{deloc}$ transitions associated with π-delocalization between the two rings, as discussed above. As demonstrated above for biphenyl and benzene, subtraction of twice the C 1s spectrum of hexafluorobenzene from that of decafluorobiphenyl gives a weak peak at 289.5 eV, which can be assigned to the C 1s → $1\pi^*_{deloc}$ transition (result not shown). The computed oscillator strengths for 60°-twisted decafluorobiphenyl (Table 3) predict that C 1s

TABLE 4: Energies (E, eV), Term Values (eV), and Assignments of Features in the C 1s and F 1s ISEELS Spectra of Hexafluorobenzene and Decafluorobiphenyl (2)

C_6F_6		**2**		assignment (final orbital)	
E	TV	E	TV	C−F	C−C
			C 1s		
		286.02[a]	6.5		1π*
287.9	6.2	287.83	6.0	1π*	
289.0	5.1	289.1	4.7	σ*(C−F)	
		289.5		π^*_{deloc}	
291.0	3.1	291.9	1.9	2π*	
292.4	1.7	293.4	0.4	3p	
293.6	0.5			4p	
		292.5[c]			IP
294.1[b]		293.8[c]		IP	
		294.0	−0.2		
295.8	−1.7	296.2	−2.4	σ*(C−C) (ring)	
298.7	−4.6	299.5	−5.7	σ*(C−C) (ring)	
304.9	−10.8	305.2	−11.4	σ*(C−C) (ring)	
			F 1s		
		687.0	7.3	1π*	
689.2	5.0	689.2[d]	5.1	σ*(C−F)	
692.0	2.2	692.1	2.2	σ*(C−F)/2π*	
693.9	0.3	693.5	0.8	σ*(C−F)	
694.2[e]		694.3[e]		IP	
697.4	−3.2	697.5	−3.2	σ*(C−F)	

[a] Calibration: −1.38(7) eV relative to the C 1s → π* transition of CO (287.40(2) eV.[50] [b] C 1s IP of C_6F_6 is taken from X-ray photoelectron spectroscopy.[52,53] [c] C 1s(C−F) IP of $C_{12}F_{10}$ was estimated by adding, to the experimental C_6F_6 IP, the weighted average of the GSCF3 computed shifts relative to the computed C_6F_6 IP. The C 1s(C−C) IP of $C_{12}F_{10}$ is estimated by adding the C−C to C−F computed shift to the C 1s(C−F) IP. [d] Calibration: −155.0(1) eV relative to the O 1s → π* transition of CO (534.21(9) eV[50]). [e] F 1s IP of $C_{12}F_{10}$ was estimated according to the same shift as calculations with respect to C_6F_6. The calculated F IP of $C_{12}F_{10}$ takes the weighted average of the values of three different sites.

→ 1π* transitions are intense for C 1s excitation to 1π*(b_1), and there is some intensity for excitation to 1π*(b_3), but the excitations to 1π*(a) and 1π*(b_2) are relatively weak. As with biphenyl, the 1π*(b_2) and 1π*(a) MOs are very close in energy. The calculations indicate that the C_2, C_3, and C_4 1s core level IPs are similar. The induction effect from the other phenyl ring is not strong enough to separate the C_3 1s level from those of C_2 and C_4, so the C 1s → 1π* transitions associated with the C_2, C_3, and C_4 sites overlap. Thus, sensitivity to the conformation and the extent of ring−ring delocalization arises from changes in the unoccupied energy levels and can be detected by ISEELS or NEXAFS, but core level photoelectron spectroscopy is not expected to be very sensitive to ring−ring delocalization.

The peak at 291.9 eV is assigned to C 1s(C−F) → 2π* transitions for decafluorobiphenyl and hexafluorobenzene.[29] Other features in the C 1s spectrum of decafluorobiphenyl are assigned to excitations to Rydberg and σ*(C−C) (ring) states by comparison with the spectra of benzene, biphenyl, hexafluorobenzene, and to the GSCF3 calculations.

3.4. F 1s Spectra of Hexafluorobenzene and Decafluorobiphenyl. Figure 8 presents the F 1s oscillator strength spectra of hexafluorobenzene and decafluorobiphenyl (**2**) derived from dipole-regime ISEELS. Figure 8 also presents for comparison, the calculated F 1s spectra of hexafluorobenzene and 60°-twisted decafluorobiphenyl. The energies, term values, and proposed assignments of the spectral features are presented in Table 3. Selected details of the F 1s calculations are presented in Table 5. Table S4 of the Supporting Information is a more extensive listing of the information from the GSCF3 calculations. The

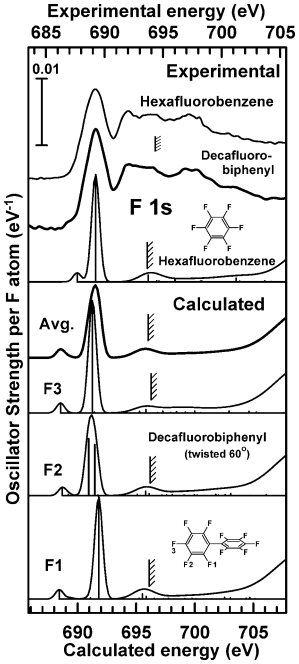

Figure 8. (Upper) F 1s oscillator strength spectra of hexafluorobenzene and decafluorobiphenyl derived from dipole regime ISEELS. (Lower) Calculated F 1s spectra of hexafluorobenzene and the 60°-twisted conformation of decafluorobiphenyl. The hatched lines indicate the IPs. The energy scale for the calculated spectra has been shifted by −2.3 to align the main σ*(C−F) feature with its experimental counterpart.

calculated spectrum is a weighted sum of calculated spectra for each of the three chemically distinct fluorine sites. The assignments of the spectral features are based on GSCF3 calculations and comparison to those for the spectrum of hexafluorobenzene.[29] F 1s term values for experiment and calculations are similar, and the spectral assignments follow from the calculations. The F 1s → 1π* transitions are symmetry allowed but are expected (and calculated) to be very weak due to limited spatial overlap of the F 1s and C 2pπ orbitals. They probably give rise to the weak shoulder at 687 eV in **2**, since this feature is not observed in the spectrum of hexafluorobenzene. The strong peak at 689.2 eV is attributed to F 1s → σ*(C−F) transitions.

3.5. C 1s Spectrum of 2,2′-Bis(bromomethyl)-1,1′-biphenyl. The oscillator spectrum for C 1s excitation of 2,2′-bis(bromomethyl)-1,1′-biphenyl (**3**) derived from dipole-regime ISEELS is presented in Figure S1 of the Supporting Information. The energies, term values, and proposed assignments for the spectral features are listed in Table 2. The mean torsional angle of this molecule was determined to be 76.3° in the solid phase by X-ray diffraction.[48] Since the bromomethyl substituents on the phenyl rings are quite bulky, the molecule is strongly twisted in the gas phase and should have a similar torsional angle in the gas and solid. The shapes and locations of the spectral features are similar to those of biphenyl, so the spectral assignments parallel those of biphenyl. The relative weakness for some low-intensity features and the broadening of the C 1s → σ*(C−C) features for 2,2′-bis(bromomethyl)-1,1′-biphenyl are probably due to the influence of the bromomethyl groups. The main C 1s → 1π* peak is broadened and shows a high-energy shoulder, reflecting contributions from C 1s(C−CH_2Br) → 1π* transitions, which are shifted to slightly higher energy due to the electronegativity of the CH_2Br substituent. There are significant chemical shifts among the chemically distinct sites around the phenyl rings in **3**, so there is extensive spectral overlap, and it is not possible to identify an experimental signal associated with C 1s → π^*_{deloc}

TABLE 5: Selected Eigenvalues, Oscillator Strengths, and Orbital Characters for Computed F 1s Core-excited States of 60°-Twisted Decafluorobiphenyl and Hexafluorobenzene

site	IP	character	ϵ (eV)	f (10^{-2})
		Decafluorobiphenyl Twisted 60°		
F1	694.186	$1\pi^*(b_1)$	−5.76	0.12
		$1\pi^*(a)$	−4.86	0.02
		$1\pi^*(b_3)$	−3.51	0.01
		$1\pi^*(b_2)$	−3.09	0.01
		σ^*(C−F)	−2.39	1.26
		$2\pi^*(b_1)$	1.06	0.03
		σ^*(C−F)	1.35	0.16
		σ^*(C−F)	3.57	0.04
		σ^*(C−F)	5.58	0.05
F2	694.176	$1\pi^*(b_1)$	−5.49	0.10
		$1\pi^*(a)$	−4.97	0.02
		σ^*(C−F)	−3.23	0.71
		σ^*(C−F)	−2.71	0.63
		σ^*(C−F)	−2.44	0.01
		$2\pi^*(b_1)$	0.91	0.04
		σ^*(C−F)	1.63	0.14
		σ^*(C−F)	3.90	0.05
		σ^*(C−F)	5.78	0.05
F3	694.372	$1\pi^*(b_1)$	−5.83	0.12
		$1\pi^*(a)$	−4.55	0.00
		σ^*(C−F)	−3.11	1.38
		σ^*(C−C)	−2.93	0.01
		σ^*(C−F)	−2.35	0.00
		$2\pi^*(b_1)$	0.91	0.05
		σ^*(C−F)	1.46	0.10
		σ^*(C−F)	4.07	0.08
		σ^*(C−F)	5.62	0.11
		Hexafluorobenzene		
F	694.155	$1\pi^*e_{2u}$	−5.99	0.11
		$1\pi^*e_{2u}$	−5.14	0.00
		σ^*(C−F)	−4.42	1.33
		σ^*(C−F)	0.07	0.21
		$2\pi^*(b_{2g})$	0.80	0.04
		σ^*(C−F)	0.99	0.03
		σ^*(C−F)	2.36	0.12
		σ^*(C−F)	4.65	0.06

transitions. In any case, these transitions are expected to be rather weak due to the large torsion angle.

3.6. C 1s Spectrum of Hexaphenylbenzene. The C 1s spectrum of solid hexaphenylbenzene (**4**), recorded with STXM, is shown in Figure 9, in comparison to the C 1s spectra of gaseous benzene and biphenyl. The insert is an optical density image at 285.1 eV of the region around the point from which the spectrum was acquired. The specific location (white circle) was selected as it is sufficiently thin so as to have an optical density that avoids spectral distortion by absorption saturation. The slits used were such that the energy resolution is on the order of 0.2 eV. The single-crystal structure determined by X-ray diffraction[49] shows that the peripheral phenyl rings of hexaphenylbenzene are twisted ∼65° with respect to the central ring. Thus, the general shape and locations of the C 1s spectral features are expected, and are found, to be similar to those of biphenyl. The spectral assignments (listed in Table 2) generally follow those of biphenyl. In addition to features similar to those of biphenyl, hexaphenylbenzene shows some extra features, in particular, enhanced peaks at 295.3 and 298.6 eV. These features are most likely associated with C 1s → σ^*(C−C) transitions at the six C−C bonds connecting the rings. Since the number of inter-ring carbons in hexaphenylbenzene (12/42) is almost twice that in biphenyl (2/12), spectral features associated with the inter-ring C−C bond should become more apparent. Another major difference of the spectrum of **4** compared to those of biphenyl and benzene is the relatively lower intensity for the C 1s → $1\pi^*$ transition in solid hexaphenylbenzene, as compared

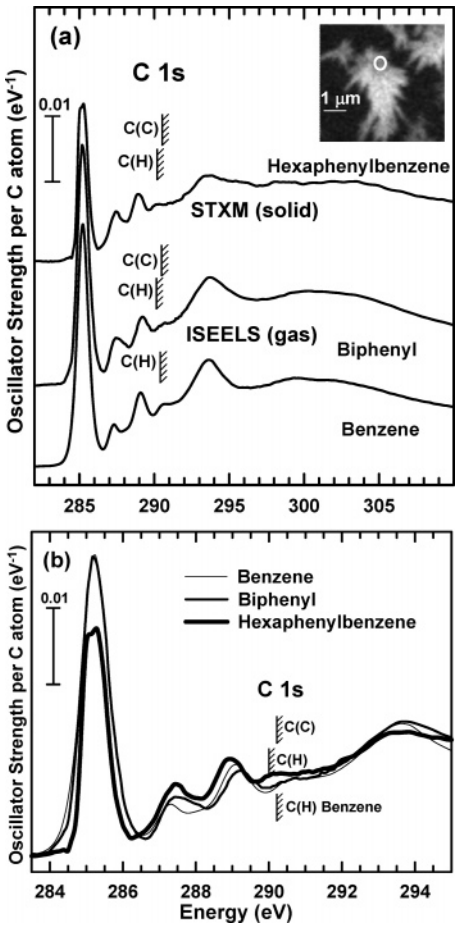

Figure 9. (a) The experimental C 1s NEXAFS spectrum of hexaphenylbenzene(s) measured in STXM. The inset is an optical density image recorded at 285.1 eV. The white circle is the area from which the spectrum was recorded. The C 1s spectra of benzene(g) and biphenyl-(g) are also plotted for comparison. The hatched lines indicate the IPs. (b) An expanded, overlap plot of the discrete region of the C 1s spectra of benzene, biphenyl, and hexaphenylbenzene.

to the C 1s continuum intensity (see Figure 9b). The explanation for this may be linear dichroism, due to the linear polarization of the light and the crystalline nature of the sample. The crystal structure is such that the hexaphenylbenzene molecules form a layer arrangement, with molecules lying in or near the (200) planes.[49] Thus, the central rings are almost parallel to each other, while the peripheral phenyl rings are twisted out from the central ring plane. In certain crystal orientations this could result in a reduced intensity for C 1s → $1\pi^*$ transitions relative to the continuum or σ^* excitations.

4. Discussion

4.1. Effect of Ring−Ring Delocalization. The spectra of biphenyl and hexaphenylbiphenyl are slightly shifted to higher energy with respect to benzene (see Figure 9b). A more precise analysis of this shift, which is most likely associated with ring−ring interaction (delocalization) can be obtained by considering the term values (see Table 2). The term values remove effects of changes in core levels and allow the discussion to focus on changes in upper level energies, where the main effects of ring−ring delocalization are expected. The term values for the $1\pi^*$ states of biphenyl, hexaphenylbenzene, and 2,2′-bis(bromomethyl)-1,1′-biphenyl are lowered by 0.3−0.4 eV compared to those of benzene. This effect is also reproduced by the GSCF3 calculations. The computed $1\pi^*$ term values of C(H) sites of

45°-twisted biphenyl (see Table 1) are lower than those of benzene by 0.1−0.3 eV.

Further inspection of the term values and the magnified $1\pi^*$ spectral region for biphenyl and hexaphenylbenzene compared to benzene (Figure 9) shows that these results are consistent with the predicted torsional angle dependence of the spectral features. Biphenyl (torsional angle of 45°) shows slightly lower π^* term values than those of hexaphenylbenzene (torsional angle of ∼65°) and 2,2′-bis(bromomethyl)-1,1′-biphenyl (torsional angle of ∼75°). The torsional angle of hexaphenylbenzene is larger than that of biphenyl by ∼20°, consistent with an increase in term values. The above analysis indicates that, although ring−ring interaction is quite small in the twisted biphenyl systems, its effects are still detectable in inner shell excitation spectra.

Both the experimental and calculated C 1s spectra of decafluorobiphenyl shift to higher energy with respect to hexafluorobenzene (Figure 7). A consideration of term values (Tables 3 and 4) indicates the π^* features of decafluorobiphenyl are lowered by 0.2−1.2 eV. These shifts are consistent with those predicted by the GSCF3 calculation (Table 3).

4.2. The Perfluoro Effect. A strong perfluoro effect was observed in perfluorinated alkanes, alkenes, and benzenes[28,29] relative to their nonfluorinated counterparts. The comparison of hexafluorobenzene and benzene (Tables 2 and 4) illustrates the effect of fluorination on IPs and transition energies. The C 1s(C−F) IP of hexafluorobenzene is 3.8 eV higher than the C 1s(C−C) IP of benzene. However the C 1s(C−F) → $1\pi^*$ transition of hexafluorobenzene is only 2.7 eV above the C 1s-(C−H) → $1\pi^*$ transition of benzene. Correcting for the core level shifts, one finds that the $1\pi^*$ level in C_6F_6 is 1.1 eV below the $1\pi^*$ level in C_6H_6. This is an example of the perfluoro effect.[30] Comparisons of other transitions indicate that analogous features in the perhydro and perfluoro molecules have similar levels of energy reduction relative to the IP shift. The GSCF3 calculations give the same trends and magnitudes for shifts in IPs, term values, and thus transition energies from benzene to hexafluorobenzene.

The perfluoro effect is also seen when comparing decafluorobiphenyl and biphenyl (Tables 2 and 4). The C 1s(C−F) IP of decafluorobiphenyl is 3.8 eV higher than that of biphenyl, whereas the C 1s(C−F) → $1\pi^*$ transition of decafluorobiphenyl is only 2.5 eV above the C 1s(C−H) → $1\pi^*$ transition of biphenyl. Again one finds that the $1\pi^*$ level in $C_{12}F_{10}$ is 1.3 eV below the $1\pi^*$ level in biphenyl. Other features have similar shifts. The GSCF3 calculations give the same trends and magnitudes for shifts in IPs, term values, and thus transition energies from biphenyl to decafluorobiphenyl (see Tables 1 and 3). The perfluoro effect on biphenyl and benzene is similar, which suggests it is likely to be similar in other aromatic compounds.

5. Summary

This paper has reported the inner shell spectra of biphenyl, decafluorobiphenyl, 2,2′-bis(bromomethyl)-1,1′-biphenyl, and hexaphenylbenzene, and interpreted them with support from ab initio GSCF3 calculations and comparisons with the spectra of related molecules, in particular, benzene and hexafluorobenzene. Energy shifts and an additional C 1s → π^*_{deloc} spectral feature are predicted, observed, and assigned to be the signature of ring−ring delocalization for biphenyl and decafluorobiphenyl, respectively. The spectral trends in molecules with different torsional angles are found to vary systematically, which may be useful in investigations of organic electronic applications involving electron transport between aromatic rings.

Acknowledgment. This research is supported financially by NSERC (Canada) and the Canadian Research Chair program. We thank Dr. Ignacio Vargas-Baca for provision of the biphenyl sample. We thank Tolek Tyliszczak and David Kilcoyne for their excellent work in developing and maintaining STXM5.3.2 at the ALS. The Advanced Light Source is funded by the Basic Energy Sciences division of the U.S. Department of Energy under contract DE-AC03-76SF00098.

Supporting Information Available: Table S1 lists geometries for core excitation GSCF3 calculations of biphenyl, decafluorobiphenyl, benzene, and hexafluorobenzene; Table S2 lists selected eigenvalues, oscillator strengths, and orbital characters for computed core-excited states of 45°-twisted biphenyl and benzene; Table S3 lists selected eigenvalues, oscillator strength, and orbital characters for computed C 1s core-excited states of 60°-twisted decafluorobiphenyl and hexafluorobenzene; Table S4 lists selected eigenvalues, oscillator strength, and orbital characters for computed F 1s core-excited states of 60°-twisted decafluorobiphenyl and hexafluorobenzene. Figure S1 shows the C 1s oscillator strength spectrum of gaseous 2,2′-bis(bromomethyl)-1,1′-biphenyl. This meterial is available free of charge via the Internet at http://pubs.acs.org.

References and Notes

(1) Kaufler, A. *Liebigs Ann. Chem.* **1907**, *351*, 151.
(2) Adams, R.; Yuan, H. C. *Chem. Rev.* **1933**, *12*, 261.
(3) Almeningen, A.; Bastiansen, O.; Fernholt, L.; Cyvin, B. N.; Cyvin, S. J.; Samdal, S. *J. Mol. Struct.* **1985**, *128*, 59.
(4) Tsuzuki, S.; Tanabe, T. *J. Phys. Chem.* **1991**, *95*, 139.
(5) Karpfen, A.; Choi, C. H.; Kertesa, M. *J. Phys. Chem. A* **1997**, *101*, 7426.
(6) Arulmozhiraja, S.; Fujii, T. *J. Chem. Phys.* **2001**, *115*, 10589.
(7) Grein, F. *J. Phys. Chem. A* **2002**, *106*, 3823.
(8) Grein, F. *J. Mol. Struct. (THEOCHEM)* **2003**, *624*, 23.
(9) Sancho-Garcia, J. C.; Cornil, J. *J. Chem. Phys.* **2004**, *121*, 3096.
(10) Eaton, V. J.; Steele, D. *J. Chem. Soc., Faraday Trans.* **1973**, *2*, 1601.
(11) Charbonneau, G.-P.; Delugeard, Y. *Acta Crystallogr. B* **1976**, *32*, 1420.
(12) Huang, C.-G.; Beveridge, K. A.; Wan, P. *J. Am. Chem. Soc.* **1991**, *113*, 7676.
(13) Im, H. S.; Bernstein, E. R. *J. Chem. Phys.* **1988**, *88*, 7337.
(14) Solak, A. O.; Ranganthan, S.; Itoh, T.; McCreery, R. L. *Electrochem. Solid State Lett.* **2002**, *5*, E43.
(15) Frey, S.; Stadler, V.; Heister, K.; Eck, W.; Zharnikov, M.; Grunze, M. *Langmuir* **2001**, *17*, 2408.
(16) Zharnikov, M.; Grunze, M. *J. Phys. Cond. Mater.* **2001**, *13*, 11333.
(17) Zubavichus, Y.; Zharnikov, M.; Yang, Y.; Fuchs, O.; Umbach, E.; Heske, C.; Ulman, A.; Grunze, M. *Langmuir* **2004**, *20*, 11022.
(18) Bauer, E. *J. El. Spec. Relat. Phenom.* **2001**, *114−116*, 975.
(19) Ade, H. In *Experimental Methods in the Physical Sciences*; Samson, J. A. R., Ederer, D. L., Eds.; Academic Press: New York, 1998; Vol. 32, p 225.
(20) Ade, H.; Urquhart, S. G. In *Chemical Applications of Synchrotron Radiation*; Sham, T. K., Ed.; World Scientific Publishing: River Edge, NJ, 2002.
(21) Stöhr, J. *NEXAFS Spectroscopy*; Springer Tracts in Surface Science: Berlin, 1992; Vol. 25.
(22) Hitchcock, A. P.; Mancini, D. C. *J. El. Spec. Relat. Phenom.* **1994**, *67*, 1. (updates of this bibliography and associated database of core excitation spectra can be accessed at http://unicorn.mcmaster.ca/corex.html).
(23) Hitchcock, A. P. *J. El. Spec. Relat. Phenom.* **2000**, *112*, 9.
(24) Minkov, I.; Gel'mukhanov, F.; Ågren, H.; Friedlein, R.; Suess, C.; Salaneck, W. R. *J. Phys. Chem. A* **2005**, *109*, 1330.
(25) Francis, J. T.; Hitchcock, A. P. *J. Phys. Chem.* **1994**, *98*, 3650.
(26) Turci, C. C.; Urquhart, S. G.; Hitchcock, A. P. *Can. J. Chem.* **1996**, *74*, 851.
(27) Gordon, M. L.; Cooper, G.; Araki, T.; Morin, C.; Turci, C. C.; Kaznatcheev, K.; Hitchcock, A. P. *J. Phys. Chem. A* **2003**, *107*, 6144.
(28) Robin, M. B.; Ishii, I.; McLaren, R.; Hitchcock, A. P. *J. Electron. Spectrosc. Relat. Phenom.* **1988**, *47*, 53.
(29) Hitchcock, A. P.; Fischer, P.; Gedanken, A.; Robin, M. B. *J. Phys. Chem.* **1987**, *91*, 531.
(30) Robin M. B. *Higher Excited States of Polyatomic Molecules*; Academic Press: New. York, 1985; Vol. 3.

(31) Kosugi, N.; Kuroda, H. *Chem. Phys. Lett.* **1980**, *74*, 490.
(32) Kosugi, N. *Theor. Chim. Acta* **1987**, *72*, 149.
(33) Horsley, J. A.; Stöhr, J.; Hitchcock, A. P.; Newbury, D. C.; Johnson, A. L.; Sette, F. *J. Chem. Phys.* **1985**, *83*, 6099.
(34) Henke, B. L.; Gullikson, E. M.; Davis, J. C. *At. Data Nucl. Data Tables* **1993**, *54*, 181.
(35) Fieser, L. F. *Org. Synth.* **1973**, *5*, 604.
(36) Kilcoyne, A. L. D.; Tyliszczak, T.; Steele, W. F.; Fakra, S.; Hitchcock, P.; Franck, K.; Anderson, E.; Harteneck, B.; Rightor, E. G.; Mitchell, G. E.; Hitchcock, A. P.; Yang, L.; Warwick, T.; Ade, H. *J. Sync. Radiat.* **2003**, *10*, 125.
(37) Warwick, T.; Ade, H.; Kilcoyne, A. L. D.; Kritscher, M.; Tyliscczcak, T.; Fakra,S.; Hitchcock, A. P.; Hitchcock, P.; Padmore, H. A. *J. Sync. Radiat.* **2002**, *9*, 254.
(38) Hitchcock, A. P.; Morin, C.; Zhang, X.; Araki, T.; Dynes, J. J.; Stover, H.; Brash, J. L.; Lawrence, J. R.; Leppard, G. G. *J. Electron. Spectrosc. Relat. Phenom.* **2005**, *144*−*147*, 259.
(39) Jacobsen, C.; Wirick, S.; Flynn, G.; Zimba, C. *J. Micros.* **2000**, *197*, 173.
(40) Huzinaga, S.; Andzelm, J.; Klobokowski, M.; Radzio-Andzelm, E.; Sasaki, Y.; Tatewaki H. *Gaussian Basis Sets for Molecular Calculations*; Elsevier: Amsterdam, 1984.
(41) Bastiansen, O.; Samdal, S. *J. Mol. Struct.* **1985**, *128*, 115.
(42) Turci, C. C.; Urquhart, S. G.; Hitchcock, A. P. *Can. J. Chem.* **1996**, *74*, 851.
(43) Rennie, E. E.; Kempgens, B.; Köppe, H. M.; Hergenhahn, U.; Feldhaus, J.; Itchkawitz, B. S.; Kilcoyne, A. L. D.; Kivimäki, A.; Maier, K.; Piancastelli, M. N.; Polcik, M.; Rüdel, A.; Bradshaw, A. M. *J. Chem. Phys.* **2000**, *113*, 7362.
(44) Shimoyama, I.; Mochida, T.; Otsuki, Y.; Horiuchi, H.; Saijyo, S.; Nakagawa, K.; Nagasono, M.; Tanaka, S.; Mase, K. J. *J. Electron. Spectrosc. Relat. Phenom.* **1988**, *88*−*91*, 791.
(45) Schwarz, W. H. E.; Chang, T. C.; Seeger, U.; Hwang, K. H. *Chem. Phys.* **1987**, *117*, 73.
(46) Gleason, W. B.; Britton, D. *Cryst. Struct. Commun.* **1976**, *5*, 483.
(47) Bastiansen, O.; Smedvik, L. *Acta Chem. Scand.* **1954**, *8*, 1593.
(48) Benmenni, L.; Alilou, E. H.; Giorgi, M.; Pierrot, M.; Réglier, M. *J. Chem. Crystallogr.* **1994**, *24*, 345.
(49) Bart, J. C. J. *Acta Crystallogr.* **1968**, *B24*, 1277.
(50) Sodhi, R. N. S.; Brion, C. E. *J. Electron. Spectrosc. Relat. Phenom.* **1984**, *34*, 363.
(51) Ohta, T.; Fujikawa, T.; Kuroda, H. *Bull. Chem. Soc. Jpn.* **1975**, *48*, 2017.
(52) Trudell, B. C.; Price, S. J. W. *Can. J. Chem.* **1977**, *55*, 1279.
(53) Davis, D. W.; Shirley, D. A.; Thomas, T. D. *Electron Spectroscopy*; North-Holland: Amsterdam, 1972; p 707.